AIP Publishing

This manuscript was accepted by Appl. Phys. Lett. Click here to see the version of record.

1 **Surfactant-induced chemical ordering of GaAsN:Bi**

2 J. Occena,[1] T. Jen,[1] H. Lu,[1] B. A. Carter,[1] T. S. Jimson,[2] A. G. Norman,[3] and R. S. Goldman[1,2*]

3 [1]*Department of Materials Science and Engineering, University of Michigan, Ann Arbor,*

4 *Michigan 48109-2136, USA*

5 [2]*Department of Physics, University of Michigan, Ann Arbor, Michigan 48109-1040, USA*

6 [3]*National Renewable Energy Laboratory, Golden, Colorado 80401, USA*

7 **September 10, 2018**

8

9 **ABSTRACT**

10 We have examined the influence of an incorporating surfactant on chemical ordering in

11 GaAsN:Bi alloys. Epitaxy with a (2x1) reconstruction leads to random GaAsN formation, while

12 the introduction of a Bi flux induces long-range chemical ordering of the {111} planes of

13 GaAsN:Bi. We propose a mechanism in which Bi enhances the formation of dimer rows aligned

14 along the [110] direction, facilitating N incorporation beneath surface dimers and Bi incorporation

15 between dimer rows to form alternating N-rich and Bi-rich {111} planes. These findings suggest

16 a route to tailoring the local atomic environment of N and Bi atoms in a wide range of emerging

17 dilute nitride-bismide alloys.

18 *Corresponding Author: rsgold@umich.edu

19

ACCEPTED MANUSCRIPT

Pursuant to the DOE Public Access Plan, this document represents the authors' peer-reviewed, accepted manuscript. The published version of the article is available from the relevant publisher.

AIP Publishing

This manuscript was accepted by Appl. Phys. Lett. Click here to see the version of record.

1 Due to the significant bandgap narrowing induced by dilute fractions of N and Bi in III-V
2 semiconductors,[1,2,3] emerging dilute nitride-bismide alloys are attractive for optoelectronic devices
3 operating in the near- to mid-infrared wavelength range. For example, the co-incorporation of N
4 and Bi in InGaAs is predicted to enable solar cells that exceed the record performance of high-
5 efficiency multi-junction photovoltaic cells.[4] In addition, the Bi-enhanced spin-orbit splitting
6 energy, combined with the N-induced lowering of the conduction band edge, is predicted to reduce
7 Auger recombination in laser diodes, enabling temperature-insensitive operation.[5,6] However, for
8 dilute nitride alloys, able carrier transport properties[7] and optical efficiencies[8] are only achieved
9 following modifications to the local N atomic configurations via thermal annealing. In addition,
10 for dilute bismide alloys, inhomogeneous broadening of spontaneous emission and modal gain
11 spectra has been attributed to variations in the local Bi atomic configuration.[9,10,11] To date, an
12 approach for long-range control of the local atomic configurations of N or Bi has yet to be reported.
13 Here, we identify the influence of an incorporating surfactant on long-range atomic configurations
14 in GaAsN:Bi, namely, long-range chemical ordering of the {111} planes. These findings suggest
15 a route for tailoring local atomic environments in a wide range of emerging dilute nitride-bismide
16 alloys and heterostructure devices.

17 Epitaxial GaAsN:Bi films were grown via nucleation and growth of two-dimensional (2D)
18 islands (i.e. layer-by-layer mode) on semi-insulating (001) GaAs substrates by molecular-beam
19 epitaxy (MBE), as described elsewhere.[12] Following oxide desorption and the growth of a 500 nm
20 thick GaAs buffer layer at 580°C, the substrate temperature was held at 580°C for 5 minutes,
21 lowered to the GaAsN:Bi growth temperature, $T_{GaAsN:Bi}$, and held at $T_{GaAsN:Bi}$ for another 5 minutes.
22 A series of films with a range of N and Bi fractions were achieved by varying the Bi beam
23 equivalent pressure (BEP) from 0 to 1.2×10^{-7} Torr (with T_{GaAsN} = 410°C and $T_{GaAsN:Bi}$ = 380°C),

Pursuant to the DOE Public Access Plan, this document represents the authors' peer-reviewed, accepted manuscript. The published version of the article is available from the relevant publisher.

ACCEPTED MANUSCRIPT

AIP Publishing
This manuscript was accepted by Appl. Phys. Lett. Click here to see the version of record.

1 which we will refer to as the "Bi flux series". In addition, a series of films with fixed Bi flux were
2 achieved by varying $T_{GaAsN:Bi}$ from 380°C to 260°C (with Bi BEP fixed at 5.7×10^{-8} Torr), which
3 we will refer to as the "T-series". The T-series consists of a multilayer structure with four 400 nm
4 GaAsN:Bi layers, each separated by 100 nm GaAs spacers. The GaAsN:Bi layers were grown in
5 order of decreasing temperature, with a temperature ramp coinciding with the growth of each
6 intervening GaAs spacer.

7 To monitor the influence of Bi flux and substrate temperature on surface reconstruction,
8 reflection high-energy electron diffraction (RHEED) patterns were collected prior to and during
9 epitaxy. For all films, streaky (2x4) patterns [Figs. 1(a) and 1(b)] were observed during the GaAs
10 buffer layer growth; the pattern transitioned to a streaky c(4x4) [Figs. 1(c) and 1(d)] during the 5
11 minute anneal at $T_{GaAsN:Bi}$. For $T_{GaAsN:Bi} < 340$°C, a streaky (1x3) pattern [Figs. 1(e) and 1(f)] was
12 observed, consistent with earlier reports for GaAsBi.[13] For $T_{GaAsN:Bi} \geq 340$°C, a streaky (2x1)
13 pattern[14] was instead observed [Figs. 1(g) and 1(h)]. For the Bi flux series, with $T_{GaAsN:Bi} = 380$°C,
14 streaky (1x3), streaky (2x1), and spotty (3x3) patterns were observed for the low, intermediate,
15 and high Bi flux values, respectively. For GaAsN growth without a Bi flux, a streaky (2x1) pattern
16 was observed [Figs. 1(k) and 1(l)].

17 Following epitaxy, the surface morphologies and compositions were examined using atomic-
18 force microscopy (AFM) and/or scanning electron microscopy (SEM), Rutherford backscattering
19 spectrometry, high-resolution x-ray diffraction, and transmission electron microscopy (TEM), as
20 described in the supplemental materials [link to be inserted]. For the Bi flux series, a set of (004)
21 x-ray rocking curves and corresponding AFM or SEM images, with Bi flux values increasing from
22 bottom to top, are shown in Fig. 2. In Fig. 2(a), Bi-flux-dependent shifts of the GaAsN:Bi peaks
23 from the high to the low angle side of the GaAs peak indicate tensile and compressive films,

Pursuant to the DOE Public Access Plan, this document represents the authors' peer-reviewed, accepted manuscript. The published version of the article is available from the relevant publisher.
ACCEPTED MANUSCRIPT

AIP Publishing

This manuscript was accepted by Appl. Phys. Lett. Click here to see the version of record.

respectively. Some of the layers exhibit coherent interference fringes, often termed Pendellösung fringes [15] which are associated with planar surfaces and well-defined epilayer-substrate interfaces.[15,16,17] For the lowest Bi flux, low-amplitude (2nm) periodic (wavelength = 40 nm) surface features [Fig. 2(c)] and correspondingly weak Pendellösung fringes are apparent. For GaAsN films and intermediate Bi fluxes, featureless surfaces, with RMS roughness <0.5nm, are apparent. Since the Pendellösung fringes are most prominent for intermediate Bi fluxes, we hypothesize that Bi acts as a surfactant,[18,19] enhancing layer-by-layer growth. For the intermediate Bi fluxes, layer-by-layer growth is also suggested by the streaky RHEED patterns [Figs. 1(g) and 1(h)]. For the highest Bi flux, a significantly broadened epilayer peak is observed, likely related to the presence of surface droplets and islands, as shown in Fig. 2(f).

We now focus on the intermediate Bi flux (y_{Bi} = 0.020 and y_{Bi} = 0.049) layers with prominent Pendellösung fringes, which we term the tensile and compressive GaAsN:Bi layers. In Fig. 3, we present ω-2θ x-ray diffraction about the ½($1\bar{1}5$) reflections for the (a) tensile and (b) compressive GaAsN:Bi layers. The presence of the ½($1\bar{1}5$) reflection, which is a forbidden reflection for the zincblende (ZB) lattice, indicates the formation of a superstructure along the [$1\bar{1}5$] direction, likely related to long-range ordering of ($1\bar{1}1$) planes.[20] We use the diffraction peak broadening to estimate ordered domain sizes of 6 nm and 5 nm along the <115> directions for the tensile and compressive GaAsN:Bi layers.[20,21] Similar sizes of ordered domain have been reported for GaInP alloys grown in the layer-by-layer mode on nominally flat (001) GaAs substrates.[20] On the other hand, ordered domain sizes >100 nm have been reported for GaInP grown in step-flow mode on 6°(111)B offcut substrates.[22]

Further quantification of chemical ordering is obtained from selected-area diffraction (SAD) patterns for the compressive GaAsN:Bi layer. For the [110] SAD pattern shown in Fig. 3(c), {002},

Pursuant to the DOE Public Access Plan, this document represents the authors' peer-reviewed, accepted manuscript. The published version of the article is available from the relevant publisher.

ACCEPTED MANUSCRIPT

AIP Publishing

This manuscript was accepted by Appl. Phys. Lett. Click here to see the version of record.

1 {111}, and {220} reflections typical of a ZB lattice are observed. In addition, ½(1$\bar{1}$1), ½(1$\bar{1}$3), and
2 ½(1$\bar{1}$5) [½($\bar{1}$11), ½($\bar{1}$13), and ½($\bar{1}$15)] superstructure reflections, indicating long-range ordering
3 on {111}B planes, i.e. $CuPt_B$ ordering,[23] are apparent. Additional [1$\bar{1}$0] SAD patterns showed only
4 the allowed ZB reflections, indicating the absence of long-range ordering on the {111}A planes,
5 i.e. a lack of $CuPt_A$ ordering. This observation of $CuPt_B$ ordering without $CuPt_A$ ordering is
6 consistent with earlier reports on GaAsBi alloys.[24,25] Assuming that the elongation of the ½(1$\bar{1}$5)
7 superstructure reflections along [001] is inversely proportional to the size of the ordered domains,[21]
8 we estimate domain sizes of 1 - 2 nm along the <001> directions for both the tensile and
9 compressive quaternary layers. For ordered GaAsBi on 2° (111)B offcut GaAs (001),[24] our
10 analysis yields larger domains, ~ 3 – 4 nm, presumably due to the enhancement of ordered domain
11 growth facilitated by the B-type[26] step-edges.[27]

12 For the T-series, AFM of the lowest-T layer (i.e. the top surface), shown in the supplemental
13 materials, [link to be inserted] reveals rms roughness <0.5 nm, suggesting layer-by-layer growth
14 throughout the structure. In the high-angle annular dark field (HAADF) scanning TEM (STEM)
15 images in Fig. 4(a), GaAsN:Bi layers are visible as bright layers separated by darker GaAs spacers.
16 For each GaAsN:Bi layer in Fig. 4(a), [110] SAD patterns are shown in Fig. 4(b)–4(e), where
17 diffraction spots for {002}, {111}, and {220} are marked with closed circles, open circles, and
18 triangles, respectively. For $T_{GaAsN:Bi}$ = 260°C and 300°C, the [110] SAD patterns show only ZB
19 reflections. For $T_{GaAsN:Bi} \geq$ 340°C, superstructure reflections appear in the ½(1$\bar{1}$1) and ½($\bar{1}$11)
20 positions, as indicated by arrows in Figs. 4(d) and 4(e), consistent with the presence of $CuPt_B$
21 ordering.[23] Additional [1$\bar{1}$0] SAD patterns show only ZB reflections, indicating a lack of $CuPt_A$
22 ordering.

Pursuant to the DOE Public Access Plan, this document represents the authors' peer-reviewed, accepted manuscript. The published version of the article is available from the relevant publisher.

ACCEPTED MANUSCRIPT

AIP Publishing

This manuscript was accepted by Appl. Phys. Lett. Click here to see the version of record.

1 We now present direct observations of the chemically ordered regions (i.e. domains) in real
2 space. In Fig. 5(a), we show a [110] cross-sectional HAADF STEM image collected near the
3 interface between GaAs and ordered GaAsN:Bi. In Fig. 5(a), the cyan and magenta arrows indicate
4 example $(1\bar{1}1)$ and $(\bar{1}11)$ planes with doubled periodicity in the $[1\bar{1}1]$ and $[\bar{1}11]$ directions. To
5 determine the ordered domain variants and size distributions, we considered several HAADF
6 STEM images, spanning an area >4000 nm^2. For each HAADF STEM image, fast Fourier
7 transforms (FFTs) reveal spots due to the ZB lattice and spots at the ½$(1\bar{1}1)$ and ½$(\bar{1}11)$ positions,
8 indicating doubled periodicities in the $[1\bar{1}1]$ and $[\bar{1}11]$ directions. We selected each conjugate pair
9 of ½$(1\bar{1}1)$ and ½$(\bar{1}11)$ spots, circled in cyan and magenta, respectively, in Fig. 5(b), and performed
10 inverse FFTs to emphasize the $(1\bar{1}1)$ and $(\bar{1}11)$ ordered domains. For each resulting Fourier-
11 filtered image, we included pixels near the top (18 ± 6%) and bottom (18 ± 7%) of the total
12 grayscale range, with thresholds selected to exclude GaAs regions. In the example Fourier-filtered
13 image shown in Fig. 5(c), both domain types are narrowed in the [001] direction and elongated
14 along the $[1\bar{1}0]$ direction, consistent with the [001] elongation of the ½$(1\bar{1}1)$ and ½$(\bar{1}11)$
15 reflections shown in Fig. 3(c), Fig. 4(d), and Fig. 4(e). Figure 5(d) shows a logarithmic-normal
16 (lognormal) fit to the domain size distribution, which yields a median domain size of 1.81 ± 0.01
17 nm^2. Using this Fourier-filtering analysis, we analyzed the high-resolution TEM image of ordered
18 GaAsBi from Fig. 4 in Ref. 25 and observed similarly-shaped domains; a lognormal fit in that case
19 yields a median domain size of 1.8 ± 0.1 nm^2. Both lognormal size distributions are consistent with
20 a domain nucleation and growth process without significant coarsening,[28] as expected for a
21 surface-driven process.

22 The appearance of both $(1\bar{1}1)$ and $(\bar{1}11)$ domains on the nominally flat substrates is likely
23 related to the growth mode. During layer-by-layer growth, step propagation proceeds away from

Pursuant to the DOE Public Access Plan, this document represents the authors' peer-reviewed, accepted manuscript. The published version of the article is available from the relevant publisher.

ACCEPTED MANUSCRIPT

AIP Publishing
This manuscript was accepted by Appl. Phys. Lett. Click here to see the version of record.

1 each 2D island, in both the $[\bar{1}10]$ and $[1\bar{1}0]$ directions. Thus, $(\bar{1}11)$ and $(1\bar{1}1)$ domains will meet
2 when adjacent islands merge, limiting the lateral size of each. In contrast, on surfaces with offcuts
3 toward (111)B, step-flow growth occurs along the B-type step edges; i.e. the $[\bar{1}10]$ or $[1\bar{1}0]$
4 directions, leading to the formation of large single-variant domains.[27]

5 In Fig. 6, the surface reconstructions for ordered and disordered GaAsN:Bi alloys are shown
6 on a plot of Bi BEP vs $T_{GaAsN:Bi}$. The dashed lines are guides to the eye, enclosing a window in
7 which *both* a (2x1) reconstruction and CuPt ordering are observed. Above the window, a spotty
8 (3x3) reconstruction, with Bi incorporated into surface droplets, shown in Fig. 2(g), is observed.
9 Below the window, disordered alloys are observed, including GaAsN and GaAsN:Bi layers grown
10 with (2x1) and (1x3) reconstructions, respectively. Interestingly, for GaAsN growth with a (2x1)
11 reconstruction, but *without* a Bi flux, ordering is not observed. Therefore, it is likely the GaAsN
12 (2x1) lacks sufficient dimer alignment for ordering;[27] however, in the presence of an incorporating
13 surfactant, Bi, the alignment of dimer rows is enhanced. Indeed, the well-defined 2x pattern
14 observed in the (2x1) pattern for GaAsN:Bi films (Fig. 1(g) and 1(h)) compared to that of GaAsN
15 films (Fig. 1(k) and 1(l)) supports this hypothesis.

16 We now present an atomistic mechanism for chemical ordering in GaAsN:Bi. For GaAsN:Bi,
17 we recently reported that up to 30% of N atoms incorporate non-substitutionally, predominantly
18 in the form of $(N\text{-}As)_{As}$ complexes.[12] Thus, the group V sublattice may be occupied by As, Bi,
19 substitutional N, or $(N\text{-}As)_{As}$. Due to its relatively high concentration ($x_{As} > 0.92$), arsenic is
20 necessarily incorporated both between and beneath dimer rows. Thus, we hypothesize that the
21 largest species, Bi, is primarily incorporated between dimer rows due to local tensile strain, while
22 the smallest species, N, tends to incorporate beneath dimer rows due to local compressive
23 strain,[27,29] forming a monolayer superlattice consisting of alternating Bi-rich and N-rich $(\bar{1}11)$

ACCEPTED MANUSCRIPT

Pursuant to the DOE Public Access Plan, this document represents the authors' peer-reviewed, accepted manuscript. The published version of the article is available from the relevant publisher.

AIP Publishing

This manuscript was accepted by Appl. Phys. Lett. Click here to see the version of record.

1 planes, as illustrated in Fig. 7, in which Bi-rich planes are highlighted in red, and N-rich planes
2 are highlighted in blue. In addition, a significant portion of the N atoms would share sites with As
3 as $(N\text{-}As)_{As}$ complexes.[12] Further work is required to determine whether these complexes are
4 incorporated between or beneath the dimer rows.

5 In summary, we have examined the influence of an incorporating surfactant on chemical
6 ordering of GaAsN:Bi during MBE. We show that CuPt ordering is tied to the presence of *both*
7 the incorporating surfactant, Bi, and a (2x1) surface reconstruction. We propose a modified dimer-
8 induced strain mechanism in which Bi enhances the formation of dimer rows aligned along the
9 [110] direction, thereby facilitating N incorporation beneath surface dimers and Bi incorporation
10 between dimer rows to form alternating N-rich and Bi-rich {111} planes. The ordered GaAsN:Bi
11 consists of intersecting $(1\bar{1}1)$ and $(\bar{1}11)$ ordered domains with a lognormal size distribution,
12 consistent with domain formation at surface steps without subsequent coarsening. These findings
13 suggest a route for tailoring local atomic environments through long-range chemical ordering in a
14 wide range of emerging dilute nitride-bismide alloys and heterostructure devices.
15
16 SUPPLEMENTAL MATERIALS
17 See the supplemental materials for details of the characterization methods.
18
19 ACKNOWLEDGEMENTS
20 We gratefully acknowledge support from the National Science Foundation (NSF Grant No.
21 DMR 1410282 and DMR 1810280), the U.S. Department of Energy (DoE) under Contract No.
22 DE-AC36-08GO28308 with the National Renewable Energy Laboratory, and the U.S. DoE Office
23 of Science Graduate Student Research Program. The authors acknowledge the assistance of the

ACCEPTED MANUSCRIPT

Pursuant to the DOE Public Access Plan, this document represents the authors' peer-reviewed, accepted manuscript. The published version of the article is available from the relevant publisher.

AIP Publishing

This manuscript was accepted by Appl. Phys. Lett. Click here to see the version of record.

1 staff at the Michigan Ion Beam Laboratory and the Michigan Center for Materials
2 Characterization, $(MC)^2$, at the University of Michigan. The JEOL 3100 electron microscope at
3 $(MC)^2$ is supported by NSF Grant No. DMR 0723032.

4

5

6 FIGURE CAPTIONS

7 FIG. 1. Reflection high-energy electron diffraction patterns collected during epitaxy of GaAsN:Bi.
8 Patterns are shown along the [110] and [1$\bar{1}$0] directions in [(a), (b)], [(e), (f)], [(g), (h)], [(i), (j)],
9 and [(k), (l)] and along the [100] and [010] directions in [(c), (d)]. [(a), (b)] streaky (2x4) pattern
10 during GaAs growth at 580°C; [(c), (d)] streaky c(4x4) pattern during annealing at $T_{GaAsN:Bi}$; [(e),
11 (f)] streaky (1x3) pattern during GaAsN:Bi growth at low $T_{GaAsN:Bi}$ or low Bi beam equivalent
12 pressure (BEP) values; [(g), (h)] streaky (2x1) pattern during GaAsN:Bi growth at higher $T_{GaAsN:Bi}$
13 and moderate Bi BEP values; [(i), (j)] spotty (3x3) pattern during GaAsN:Bi growth with the
14 highest Bi BEP values. [(k), (l)] nearly-streaky (2x1) pattern during GaAsN growth.

15

16 FIG. 2: Plot of x-ray intensity versus $\Delta\omega$ for rocking curves about the GaAs (004) reflection for
17 the Bi flux series, in order of increasing Bi flux from bottom to top. For all plots, the GaAs substrate
18 peak is set to $\Delta\omega$ = 0 arcseconds; the Bi fraction, y_{Bi}, and N fraction, x_N, are displayed above each
19 curve; and corresponding atomic-force microscopy (AFM) or scanning-electron microscopy
20 (SEM) images are shown on the right. For the AFM images, the colorscale ranges displayed are
21 (b) 2nm, (c) 3 nm, (d) 2 nm, and (e) 3 nm. For the SEM image in (f), a corresponding energy-
22 dispersive x-ray spectroscopy image is shown in (g), with the blue regions consisting primarily of
23 Bi and the mottled red-green region containing Ga, As, and N.

Pursuant to the DOE Public Access Plan, this document represents the authors' peer-reviewed, accepted manuscript. The published version of the article is available from the relevant publisher.

ACCEPTED MANUSCRIPT

AIP Publishing

This manuscript was accepted by Appl. Phys. Lett. Click here to see the version of record.

ACCEPTED MANUSCRIPT

FIG. 3: Plots of x-ray intensity for ω-2θ scans about the GaAsN:Bi ½ $(1\bar{1}5)$ reflections for (a) tensile and (b) compressive GaAsN:Bi films. The presence of the ½ $(1\bar{1}5)$ reflection suggests ordering of the $(1\bar{1}1)$ planes. (c) representative [110] selected-area diffraction (SAD) pattern for the compressive GaAsN:Bi in (b), showing ½$(1\bar{1}1)$, ½$(1\bar{1}3)$, and ½$(1\bar{1}5)$ [½$(\bar{1}11)$, ½$(\bar{1}13)$, and ½$(\bar{1}15)$] reflections, indicating long-range ordering on $(1\bar{1}1)$ [$(\bar{1}11)$] planes. Additional $[1\bar{1}0]$ SAD patterns showed only ZB reflections, indicating an absence of long-range ordering on the {111}A planes. Similar SAD patterns were obtained for the tensile GaAsN:Bi.

FIG. 4: (a) High-angle annular dark field scanning transmission electron micrograph of the T-series, with alternating bright and dark layers consisting of GaAsN:Bi and GaAs, respectively. Selected-area diffraction patterns collected along the [110] zone axis for $T_{GaAsN:Bi}$ = 260°C, 300°C, 340°C, and 380°C are shown in (b) – (e), respectively. The diffraction spots for {002}, {111}, and {220} are identified by closed circles, open circles, and triangles, respectively. Arrows in (d) and (e) indicate ½$(1\bar{1}1)$ and ½$(\bar{1}11)$ reflections corresponding to $CuPt_B$ ordering.

FIG. 5: (a) High-resolution scanning transmission electron micrograph, collected near an interface between GaAs and ordered GaAsN:Bi. The magenta and cyan arrows in (a) indicate example $(\bar{1}11)$ and $(1\bar{1}1)$ planes with doubled periodicity in the $[\bar{1}11]$ and $[1\bar{1}1]$ directions, i.e. $(\bar{1}11)$ and $(1\bar{1}1)$ ordered domains. (b) Fast Fourier transform (FFT) of the image in (a), showing spots corresponding to the zincblende lattice and those at the ½$(1\bar{1}1)$ and ½$(\bar{1}11)$ positions. Inverse FFTs, using the spots circled in (b), with pixels near the top (18 ± 6%) and bottom (18 ± 7%) of the total grayscale range, are shown in (c), with magenta and cyan regions representing the $(\bar{1}11)$

Pursuant to the DOE Public Access Plan, this document represents the authors' peer-reviewed, accepted manuscript. The published version of the article is available from the relevant publisher.

AIP Publishing

This manuscript was accepted by Appl. Phys. Lett. Click here to see the version of record.

1 and $(1\bar{1}1)$ ordered domains. For both the $(\bar{1}11)$ and $(1\bar{1}1)$ ordered domains, the distribution of
2 domain sizes, fit with a logarithmic-normal (lognormal) distribution, is shown in (d).
3
4 FIG. 6: Window for $CuPt_B$ ordering in GaAsN:Bi: Bi beam equivalent pressure (BEP) vs $T_{GaAsN:Bi}$.
5 (1x3), (3x3), and (2x1) surface reconstructions are represented by squares, circles, and diamonds,
6 respectively. Solid (open) symbols denote ordered (disordered) films. The dashed lines are a guide
7 to the eye.
8
9 FIG. 7: Proposed atomistic mechanism for $CuPt_B$ ordering. White, gray, green, blue, and red circles
10 correspond to surface dimer, Ga, As, N, and Bi atoms, respectively. N and Bi atoms attach at step
11 edges flowing in the $[\bar{1}10]$ ($[1\bar{1}0]$) direction, leading to alternating N-rich/Bi-poor and N-poor/Bi-
12 rich $(\bar{1}11)$ $[(1\bar{1}1)]$ planes, highlighted by blue and red bars respectively. A fraction of N atoms
13 share As lattice sites as $(N\text{-}As)_{As}$ complexes.
14

ACCEPTED MANUSCRIPT

Pursuant to the DOE Public Access Plan, this document represents the authors' peer-reviewed, accepted manuscript. The published version of the article is available from the relevant publisher.

AIP Publishing

This manuscript was accepted by Appl. Phys. Lett. Click here to see the version of record.

1

[1] W. Shan, W. Walukiewicz, J. Ager, E. Haller, J. Geisz, D. Friedman, J. Olson, and S. Kurtz, Phys. Rev. Lett. 82, 1221 (1999).

[2] K. Alberi, J. Wu, W. Walukiewicz, K.M. Yu, O.D. Dubon, S.P. Watkins, C.X. Wang, X. Liu, Y.-J. Cho, and J. Furdyna, Phys. Rev. B 75, 051909 (2007).

[3] S. Tixier, S.E. Webster, E.C. Young, T. Tiedje, S. Francoeur, A. Mascarenhas, P. Wei, and F. Schiettekatte, Appl. Phys. Lett. 86, 112113 (2005).

[4] T. Liu, F. Suarez, A. Sukiasyan, and J. Lang, U.S. patent application 15/609,760 (21 December 2017).

[5] S.J. Sweeney and S.R. Jin, J. Appl. Phys. 113, 043110 (2013).

[6] M. Yoshimoto, W. Huang, G. Feng, Y. Tanaka, and K. Oe, J. Cryst. Growth 301–302, 975 (2007).

[7] Y. Jin, R.M. Jock, H. Cheng, Y. He, A.M. Mintarov, Y. Wang, C. Kurdak, J.L. Merz, and R.S. Goldman, Appl. Phys. Lett. 95, 062109 (2009).

[8] V. Lordi, H.B. Yuen, S.R. Bank, M.A. Wistey, J.S. Harris, and S. Friedrich, Phys. Rev. B 71, 125309 (2005).

[9] I.P. Marko, P. Ludewig, Z.L. Bushell, S.R. Jin, K. Hild, Z. Batool, S. Reinhard, L. Nattermann, W. Stolz, K. Volz, and S.J. Sweeney, J. Phys. D Appl. Phys. 47, 345103 (2014).

[10] L.C. Bannow, O. Rubel, S.C. Badescu, P. Rosenow, J. Hader, J.V. Moloney, R. Tonner, and S.W. Koch, Phys. Rev. B 93, 205202 (2016).

[11] J. Hader, S.C. Badescu, L.C. Bannow, J.V. Moloney, S.R. Johnson, and S.W. Koch, Appl. Phys. Lett. 112, 062103 (2018).

ACCEPTED MANUSCRIPT

Pursuant to the DOE Public Access Plan, this document represents the authors' peer-reviewed, accepted manuscript. The published version of the article is available from the relevant publisher.

AIP Publishing

This manuscript was accepted by Appl. Phys. Lett. Click here to see the version of record.

[12] J. Occena, T. Jen, E.E. Rizzi, T.M. Johnson, J. Horwath, Y.Q. Wang, and R.S. Goldman, Appl. Phys. Lett. 110, 242102 (2017).

[13] R.L. Field III, J. Occena, T. Jen, D. Del Gaudio, B. Yarlagadda, C. Kurdak, and R.S. Goldman, Appl. Phys. Lett. 109, 252105 (2016).

[14] W. Huang, K. Oe, G. Feng, and M. Yoshimoto, J. Appl. Phys. 98, 053505 (2005).

[15] B.W. Batterman and G. Hildebrandt, Acta Crystallograph. A 24, 150 (1968).

[16] L. Tapfer, Phys. Scripta 1989, 45 (1989).

[17] G. Mussler, J.-M. Chauveau, A. Trampert, M. Ramsteiner, L. Däweritz, and K.H. Ploog, J. Crys. Growth 267, 60 (2004).

[18] S. Tixier, M. Adamcyk, E.C. Young, J.H. Schmid, and T. Tiedje, J. Cryst. Growth 251, 449 (2003).

[19] R. Salas, S. Guchhait, K.M. McNicholas, S.D. Sifferman, V.D. Dasika, D. Jung, E.M. Krivoy, M.L. Lee, and S.R. Bank, Appl. Phys. Lett. 108, 182102 (2016).

[20] Q. Liu, W. Prost, and F.J. Tegude, Appl. Phys. Lett. 67, 2807 (1995).

[21] E. Morita, M. Ikeda, O. Kumagai, and K. Kaneko, Appl. Phys. Lett. 53, 2164 (1988).

[22] R.L. Forrest, T.D. Golding, S.C. Moss, Y. Zhang, J.F. Geisz, J.M. Olson, A. Mascarenhas, P. Ernst, and C. Geng, Phys. Rev. B 58, 15355 (1998).

[23] A. Gomyo, T. Suzuki, and S. Iijima, Phys. Rev. Lett. 60, 2645 (1988).

[24] A.G. Norman, R. France, and A.J. Ptak, J. Vac. Sci. Technol. B 29, 03C121 (2011).

[25] D.F. Reyes, F. Bastiman, C.J. Hunter, D.L. Sales, A.M. Sanchez, J.P.R. David, and D. González, Nanoscale Res. Lett. 9, 23 (2014).

[26] M.D. Pashley, K.W. Haberern, and J.M. Gaines, Appl. Phys. Lett. 58, 406 (1991).

ACCEPTED MANUSCRIPT

Pursuant to the DOE Public Access Plan, this document represents the authors' peer-reviewed, accepted manuscript. The published version of the article is available from the relevant publisher.

AIP Publishing

This manuscript was accepted by Appl. Phys. Lett. Click here to see the version of record.

[27] B.A. Philips, A.G. Norman, T.Y. Seong, S. Mahajan, G.R. Booker, M. Skowronski, J.P. Harbison, and V.G. Keramidas, J. Cryst. Growth 140, 249 (1994).

[28] R.B. Bergmann and A. Bill, J. Cryst. Growth 310, 3135 (2008).

[29] F.K. LeGoues, V.P. Kesan, S.S. Iyer, J. Tersoff, and R. Tromp, Phys. Rev.Lett. 64, 2038 (1990).

ACCEPTED MANUSCRIPT

Pursuant to the DOE Public Access Plan, this document represents the authors' peer-reviewed, accepted manuscript. The published version of the article is available from the relevant publisher.

AIP Publishing

This manuscript was accepted by Appl. Phys. Lett. Click here to see the version of record.

FIG. 1

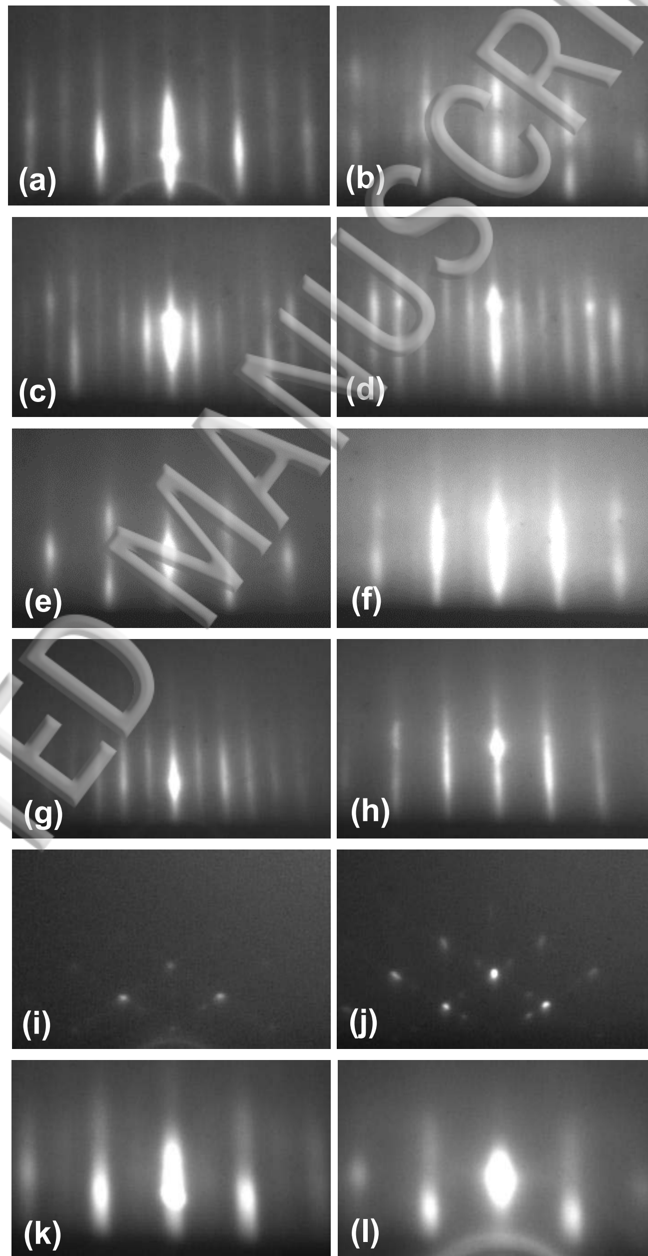

ACCEPTED MANUSCRIPT

Pursuant to the DOE Public Access Plan, this document represents the authors' peer-reviewed, accepted manuscript. The published version of the article is available from the relevant publisher.

AIP Publishing

This manuscript was accepted by Appl. Phys. Lett. Click here to see the version of record.

FIG. 2

ACCEPTED MANUSCRIPT

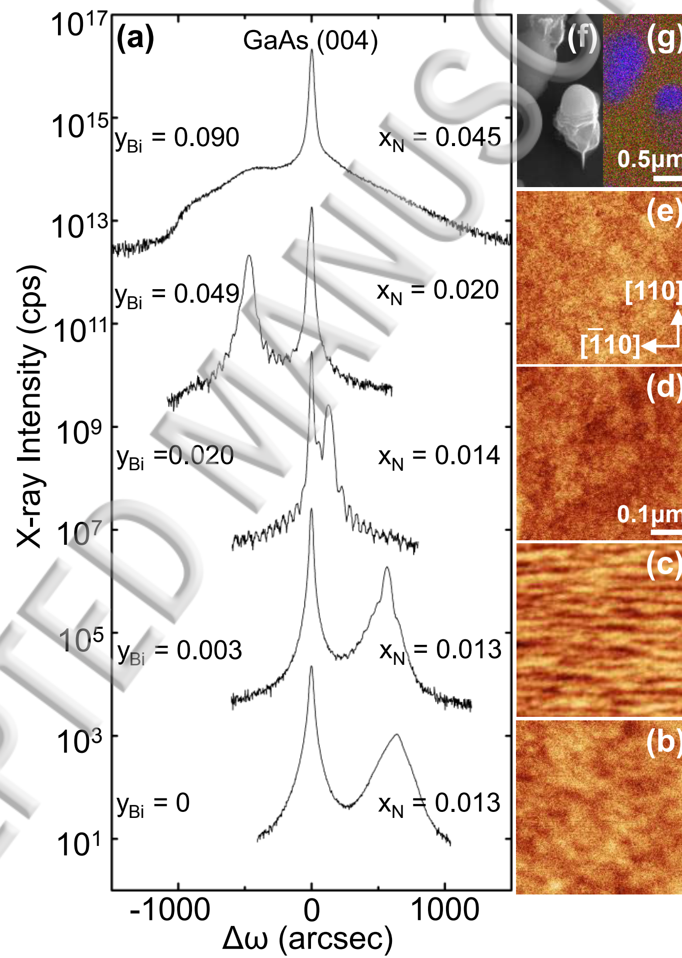

Pursuant to the DOE Public Access Plan, this document represents the authors' peer-reviewed, accepted manuscript. The published version of the article is available from the relevant publisher.

AIP Publishing

This manuscript was accepted by Appl. Phys. Lett. Click here to see the version of record.

FIG. 3

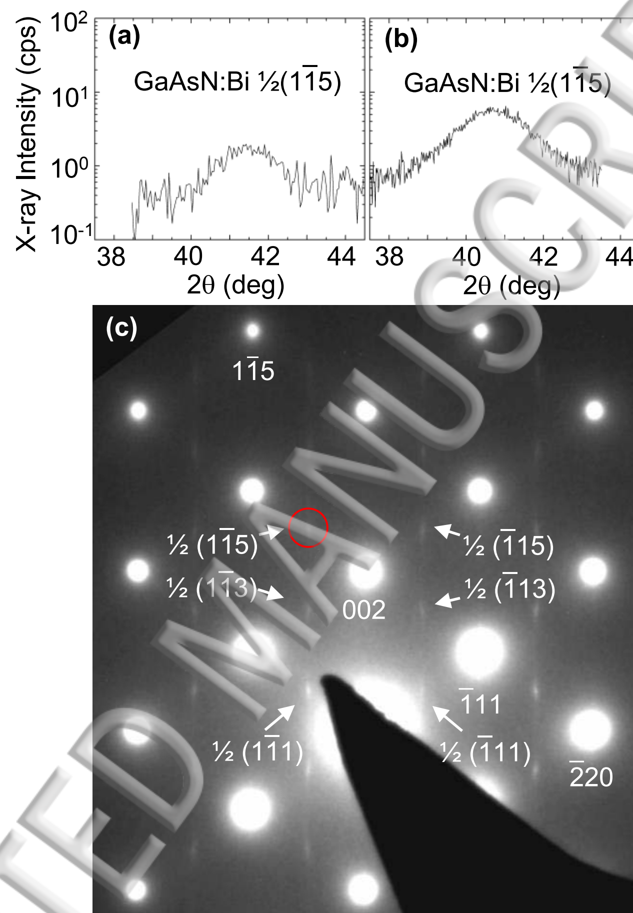

ACCEPTED MANUSCRIPT

Pursuant to the DOE Public Access Plan, this document represents the authors' peer-reviewed, accepted manuscript. The published version of the article is available from the relevant publisher.

AIP Publishing

This manuscript was accepted by Appl. Phys. Lett. Click here to see the version of record.

FIG. 4

ACCEPTED MANUSCRIPT

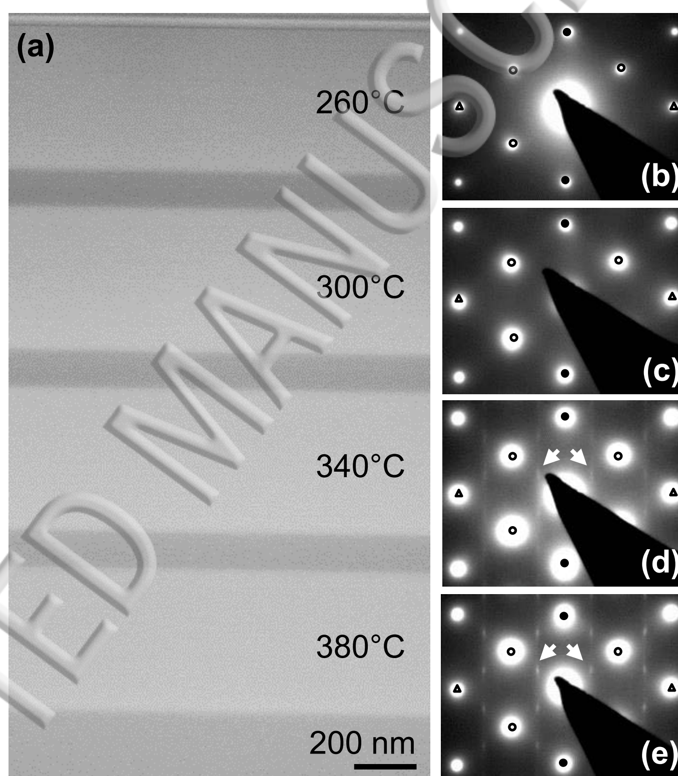

Pursuant to the DOE Public Access Plan, this document represents the authors' peer-reviewed, accepted manuscript. The published version of the article is available from the relevant publisher.

AIP Publishing

This manuscript was accepted by Appl. Phys. Lett. Click here to see the version of record.

FIG. 5

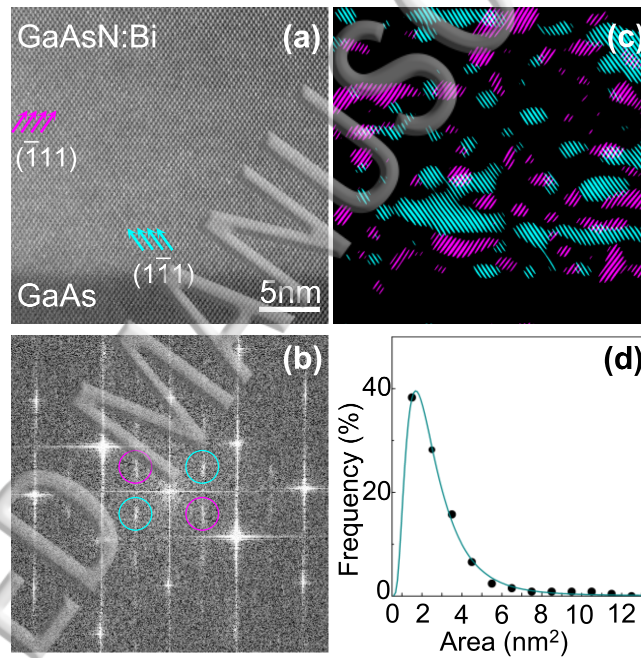

ACCEPTED MANUSCRIPT

Pursuant to the DOE Public Access Plan, this document represents the authors' peer-reviewed, accepted manuscript. The published version of the article is available from the relevant publisher.

AIP Publishing

This manuscript was accepted by Appl. Phys. Lett. Click here to see the version of record.

FIG. 6

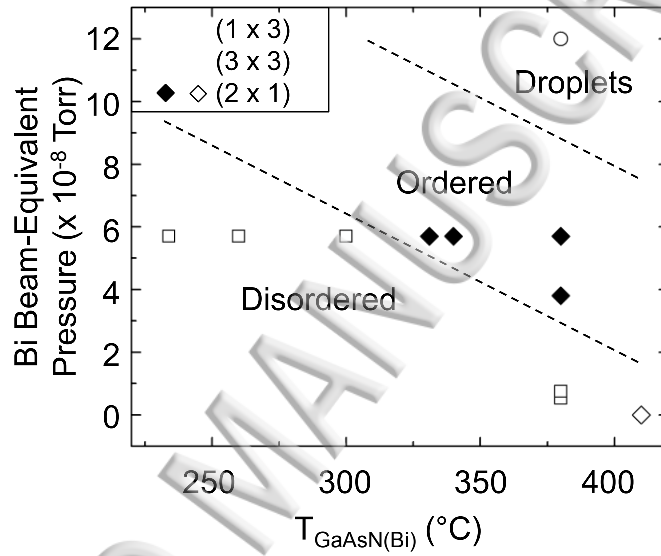

ACCEPTED MANUSCRIPT

Pursuant to the DOE Public Access Plan, this document represents the authors' peer-reviewed, accepted manuscript. The published version of the article is available from the relevant publisher.

AIP Publishing

This manuscript was accepted by Appl. Phys. Lett. Click here to see the version of record.

FIG. 7

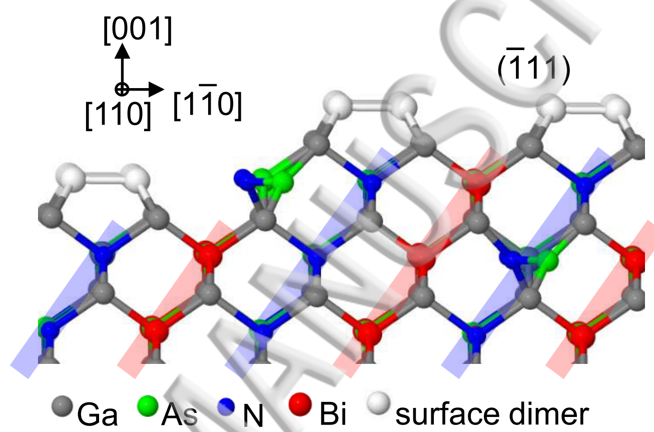

ACCEPTED MANUSCRIPT

Pursuant to the DOE Public Access Plan, this document represents the authors' peer-reviewed, accepted manuscript. The published version of the article is available from the relevant publisher.